


Modeling vanishing white matter disease with patient-derived induced pluripotent stem cells reveals astrocytic dysfunction

Ling Zhou¹  | Peng Li² | Na Chen¹ | Li-Fang Dai¹ | Kai Gao¹ | Yi-Nan Liu² | Li Shen² | Jing-Min Wang¹ | Yu-Wu Jiang¹ | Ye Wu¹

¹Department of Pediatrics, Peking University First Hospital, Beijing, China

²Department of Cell Biology, School of Basic Medical Sciences, Stem Cell Research Center, Peking University, Beijing, China

Correspondence

Ye Wu, Department of Pediatrics, Peking University First Hospital, Beijing, China.
Email: dryewu@263.net

Funding information

the construction of a clinical evaluation platform for demonstration new drug for children's rare disease, Grant/Award Number: 2017ZX09304029-006; Beijing key laboratory of molecular diagnosis and study on pediatric genetic diseases, Grant/Award Number: BZ0317; the Public Foundation of Beijing Center of Neural Regeneration and Repair; Beijing Municipal Natural Science Key Project, Grant/Award Number: 15G10050; Beijing Institute for Brain Disorders Foundation, Grant/Award Number: BIBDPXM2014_014226_000016; Beijing Municipal Science & Technology Commission, Grant/Award Number: Z16110000216133 and Z161100004916169; Clinical Medicine Plus X project of Peking University, Fundamental Research Funds for the Central Universities, Grant/Award Number: BMU2017JI002, BMU2018XY006 and PKU2017LCX06; Beijing Natural Science Foundation, Grant/Award Number: 7151010 and 7172217; National Natural Science Foundation of China, Grant/Award Number: 81741053, 81601131 and 81501123; National Key Research and Development Program of China, Grant/Award Number: 2016YFC1306201 and 2016YFC0901505

Summary

Aims: Vanishing white matter disease (VWM) is an inherited leukoencephalopathy in children attributed to mutations in *EIF2B1–5*, encoding five subunits of eukaryotic translation initiation factor 2B (eIF2B). Although the defects are in the housekeeping genes, glial cells are selectively involved in VWM. Several studies have suggested that astrocytes are central in the pathogenesis of VWM. However, the exact pathomechanism remains unknown, and no model for VWM induced pluripotent stem cells (iPSCs) has been established.

Methods: Fibroblasts from two VWM children were reprogrammed into iPSCs by using a virus-free nonintegrating episomal vector system. Control and VWM iPSCs were sequentially differentiated into neural stem cells (NSCs) and then into neural cells, including neurons, oligodendrocytes (OLs), and astrocytes.

Results: Vanishing white matter disease iPSC-derived NSCs can normally differentiate into neurons, oligodendrocyte precursor cells (OPCs), and oligodendrocytes *in vitro*. By contrast, VWM astrocytes were dysmorphic and characterized by shorter processes. Moreover, δ -GFAP and α B-Crystalline were significantly increased in addition to increased early and total apoptosis.

Conclusion: The results provided further evidence supporting the central role of astrocytic dysfunction. The establishment of VWM-specific iPSC models provides a platform for exploring the pathogenesis of VWM and future drug screening.

KEYWORDS

astrocytes, induced pluripotent stem cells, neural stem cells, neurons, oligodendrocytes, vanishing white matter disease

1 | INTRODUCTION

Human induced pluripotent stem cells (iPSCs) have the potential for self-renewal and multilineage differentiation.¹ iPSCs have been a useful tool for establishing disease-specific models for exploring the mechanisms of specific diseases by using the patients' own cells, such as dermal fibroblasts and urothelia.

Vanishing white matter disease (VWM) is one of the most prevalent inherited leukoencephalopathies in childhood and is characterized by progressive motor deterioration with episodic aggravation predisposed by stress, such as febrile infection, minor head trauma, and acute fright.²⁻⁵ The disease-causing genes are *EIF2B1-5*, encoding the subunits of eukaryotic translation initiation factor 2B (eIF2B α , β , γ , δ , and ϵ), which are responsible for the initiation of eukaryotic protein translation.⁶⁻⁹ Although the defects are in the housekeeping genes, glial cells are selectively affected in VWM. The definite mechanism of VWM remains unrevealed, and no iPSC model has been established in VWM. In this study, fibroblasts from two VWM children were reprogrammed into iPSCs for the first time by using virus-free nonintegrating episomal vector system.¹⁰⁻¹² Control and VWM iPSCs were sequentially differentiated into neural stem cells (NSCs) and then into neurons, oligodendrocytes, and astrocytes, respectively. We tried to determine whether there is a disturbance in the differentiation processes of VWM NSCs into different lineages.

2 | MATERIALS AND METHODS

2.1 | Isolation of VWM patients' dermal fibroblasts and cell culture

Human dermal fibroblasts (HDFs) from the dermis of two VWM children were used for the establishment of the VWM1-iPSCs and VWM2-iPSCs. Two age-matched control iPSCs (C1 and C2) were obtained from the Stem Cell Research Center at Peking University. The HDFs were cultured in a standard medium containing high-glucose DMEM supplemented with 10% fetal bovine serum (FBS). iPSCs were maintained in Essential 8 medium (E8, Life Technology, Carlsbad, CA, USA) on Matrigel (BD Biosciences, San Jose, CA, USA). iPSCs were passaged every 3-5 days by EDTA (Life Technology).

2.2 | Generation of VWM iPSCs from HDFs

Yamanaka episomal plasmids used in experiments, including pCXLE-hOCT3/4-SHP53 (#27-007), pCXLE-hSK (#27078), pCXLE-hUL (#27080), and pCXLE-EGFAP (#27082) (encoding OCT4, SOX2, Lin28, L-MYC, and KLF4). HDFs (5×10^5) were counted and resuspended in the Nucleofector solution supplied in the Amaxa Nucleofector kit (Lonza, Basel, Switzerland). The episomal plasmids were added to the cell suspensions at 10 μ g each per reaction and were cotransfected using the program

U-023 on the Amaxa Nucleofector device. The cells were then transferred to a Matrigel-coated 60-mm culture dish and cultured in the fibroblast medium for 3 days, and then changed to N2B27 medium supplemented with bFGF (Invitrogen, Carlsbad, CA, USA), Y-27632 (Sigma, St. Louis, MO, USA), CHIR99021 (Selleck, Houston, TX, USA), PD0325901 (Selleck), hLIF (Invitrogen), and A-83-01 (Selleck). On day 12, the medium was changed to E8. By 20-30 days post-transfection, clones were picked and cultured in E8 medium.

2.3 | Characterization of the iPSCs

Chromosomal G-band analysis was performed on VWM iPSCs with more than 10 passages. Alkaline phosphatase (ALP) staining was performed by using an ALP kit (Invitrogen). Teratoma assay was performed to test the in vivo differentiation potential of iPSCs. The undifferentiated iPSCs (1×10^7 cells/mL) were suspended in PBS and injected subcutaneously into the posterior limbs of 4-week-old NOD/SCID mice. Two months after injection, the teratomas were dissected and fixed in 4% paraformaldehyde. The paraffin-embedded tissue was sliced and stained with hematoxylin and eosin.

2.4 | RNA isolation and quantitative real-time PCR

Total RNA was extracted using Trizol reagent (Invitrogen). cDNA was synthesized using a reverse transcription kit (Promega, Madison, WI, USA). Quantitative PCR was performed using SYBR Green Real-time PCR Master Mix (Promega). The relative expression levels were normalized to those of GAPDH based on the delta-Ct method. The forward and reverse primers for real-time PCR are as follows: GAPDH (CTCTCTGCTCCTCCTGTTTCGAC, TGAGCGATGTGGCTCGGCT); Total GFAP(AGAAGCTCCAGGATGAAACC, TTCATCTGCTTCC TGCTATAGG); α -GFAP (AGAGGTCATTAAGGAGTCCA, CAACTA TCCTGCTTCTGCTC); δ -GFAP(CCTACAGGAAGCTGCTAGAG, GCG TTCCATTTACAATCTGGT).

2.5 | Immunofluorescence assay

Cells were fixed with 4% paraformaldehyde. The primary antibodies included OCT4 (1:200; Abcam, Cambridge, UK), SOX2 (1:400; CST, Danvers, MA, USA), SSEA4 (1:200; CST), MBP (1:100; Santa Cruz Biotechnology, Santa Cruz, CA, USA), GFAP (1:100; CST), S100 β (1:100; Abcam), Nestin (1:100; Abcam), Neurofilament H (1:100; CST), and β III-tubulin (1:100; CST), PDGFR α (1:100, Santa cruz), NG2 (1:100, Santa cruz), α B-Crystalline (1:200, Abcam). Secondary antibodies 488/568 goat antimouse/rabbit IgG (Invitrogen) were used and diluted at 1:500. The cell nuclei were counterstained with Hoechst33342 (Invitrogen). The labeled cells were imaged with a confocal microscope (Olympus FluoView FV10i, Tokyo, Japan).

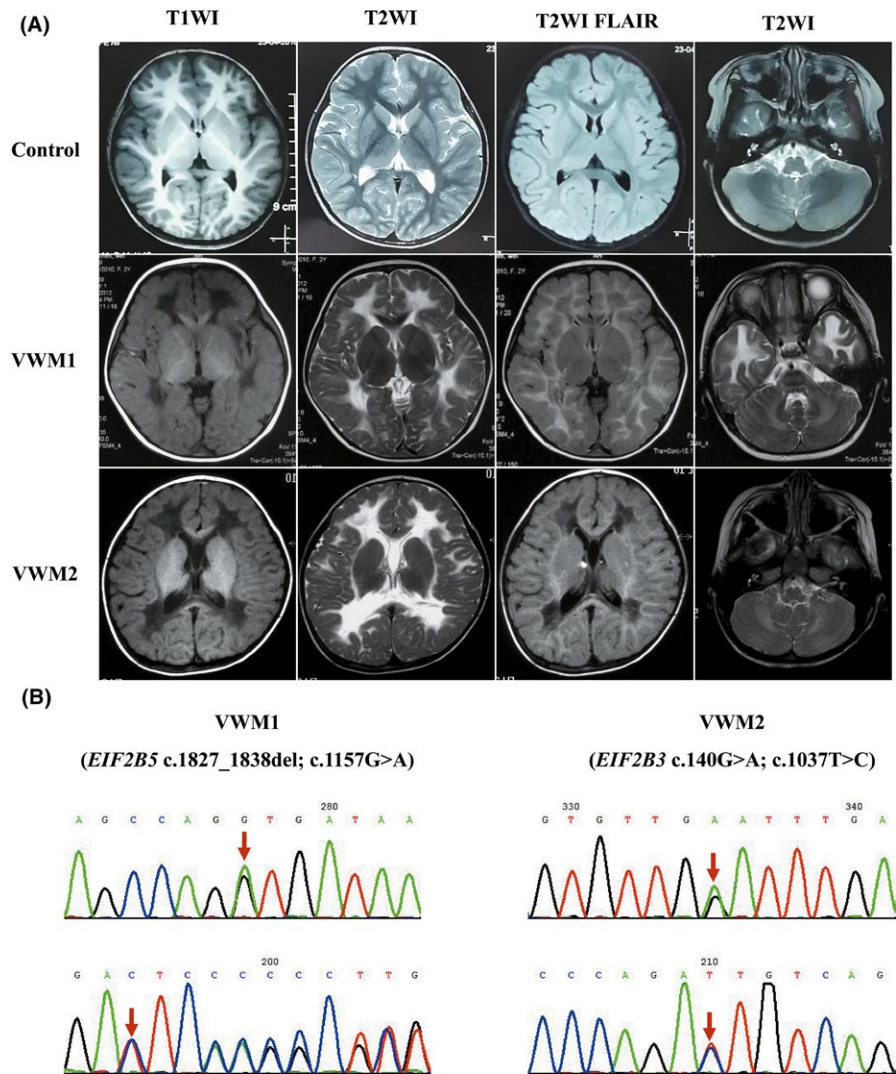


FIGURE 1 Features of the two VWM patients. a, Brain MRI of patients VWM1 and VWM2 and an age-matched control, performed at the age of 4, 3, and 4, respectively: A, E, and I (T1WI); B, D, F, K, J, and L (T2WI); C, G, and K (T2 FLAIR). Brain MRI of both VWM patients showed symmetric abnormal signals on T1WI, T2WI, and T2 FLAIR in the white matter (WM), which was partially rarefied. b, Direct sequencing analysis of the genomic DNA from the two VWM patients' iPSCs showed VWM1: *EIF2B5* c.1827_1838del (p. Ser610_Asp613del), c.1157G>A (p. Gly386Val); VWM2: *EIF2B3* c.140G>A (p. Gly47Glu), c.1037T>C (p. Ile346Thr)

2.6 | In vitro differentiation of iPSCs

Vanishing white matter disease and control iPSCs more than 10 passages were differentiated into NSCs and then sequentially differentiated into neural cells, including neurons, oligodendrocytes (OLs), and astrocytes. Markers in different differentiation stages were detected. The fluorescence density was quantitatively detected by the following method: 8-10 fields were randomly selected, including at least five areas in each field, then the mean fluorescence density in each area was calculated.

2.6.1 | Differentiation into NSCs

Induced pluripotent stem cells colonies were digested with EDTA when the iPSCs reached 70%-80% confluence and then cultured in an E8 medium for a day. For 2-7 days, the cells were cultured in a neural induction medium (Stemcell), and NSCs were formed and cultured in an NSC medium (DMEM/F12: Neural basal medium = 1:1 supplemented with $1 \times N2$, $1 \times B27$, 20 ng/mL bFGF). Immunofluorescence assay was used to detect the markers Nestin and SOX2.

2.6.2 | Differentiation into neurons

Neural stem cells were digested into single cells and then plated onto a Matrigel-coated culture dish and cultured in a neuronal medium (bFGF removed from the NSC medium). By 7 days, the markers β III-tubulin and Neurofilament H were detected.

2.6.3 | Differentiation into astrocyte lineages

Neural stem cells were dissociated into single cells using Accutase and cultured in an astrocyte differentiation medium (Stemcell), and the cells were passaged every 4 days, both Nestin and CD44, indicative of immature astrocytes, were detected by immunofluorescence assay. By 12 days, the cells were digested and cultured in an astrocyte maturation medium (Stemcell). After at least one passages, the markers of GFAP and S100 β , which are indicative of mature astrocytes, were detected by immunofluorescence assay. The number of processes and the length of the longest process from the margin of the nuclei were measured by calculating 10 randomly selected fields (cell number >5).

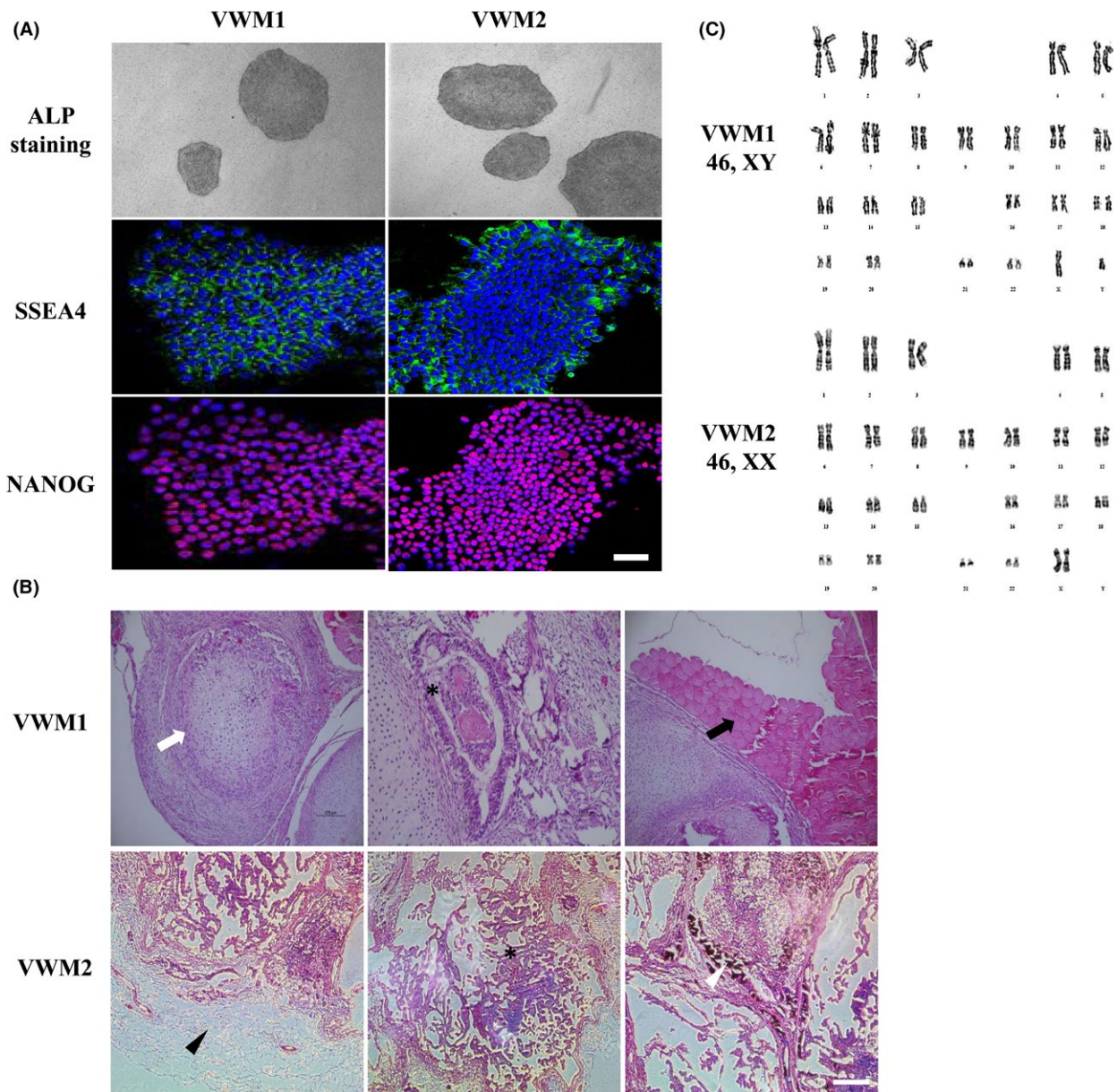


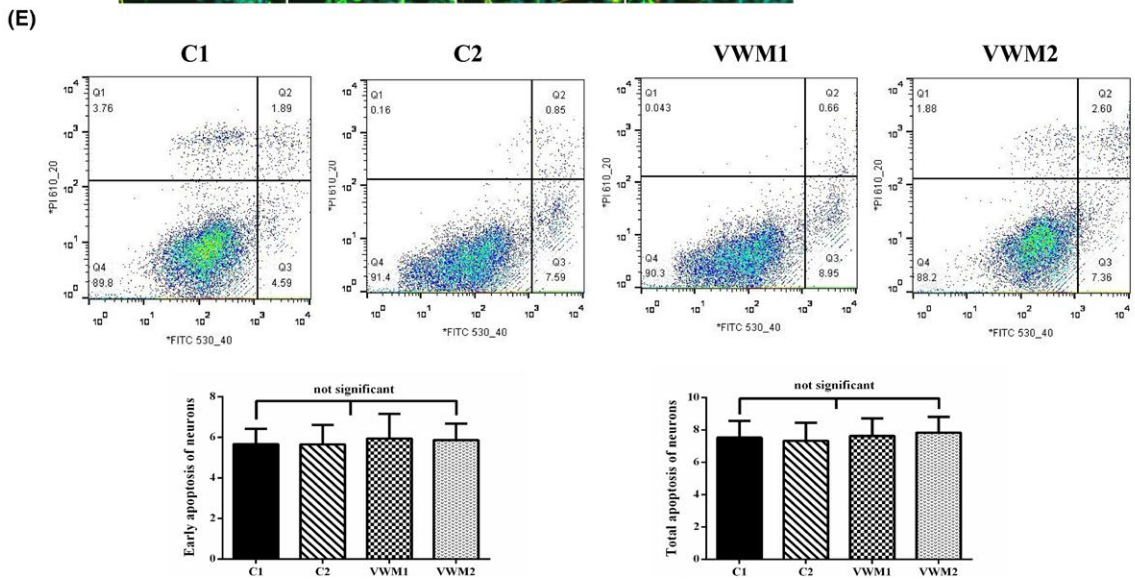
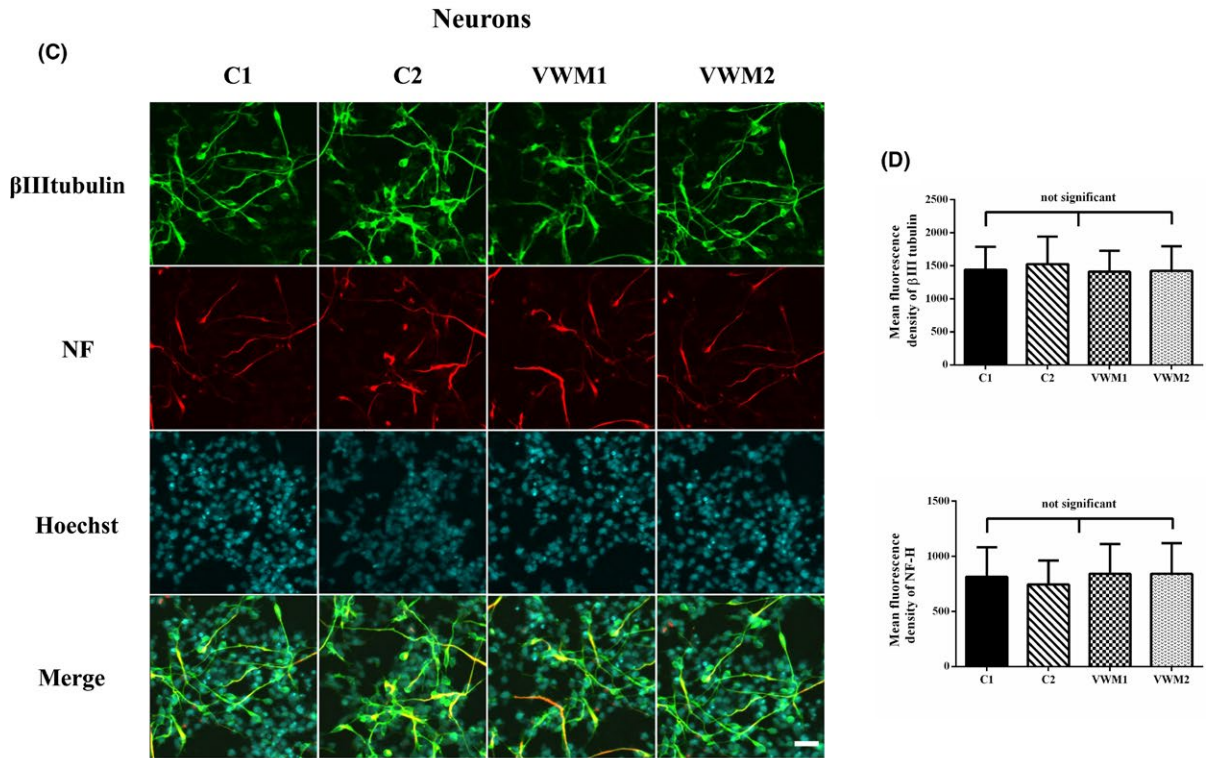
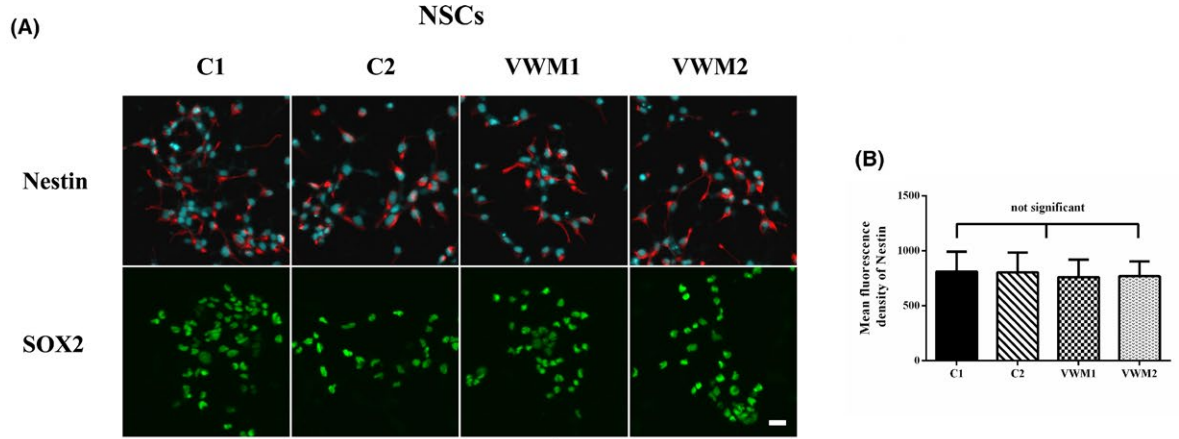
FIGURE 2 Characterization of VWM iPSCs. a, Positive alkaline phosphatase staining showed typical morphology of iPSC clones (top) and immunochemical analysis of pluripotent markers, SSEA4, and NANOG (bottom). b, Representative hematoxylin and eosin staining of teratomas derived from the established VWM iPSC clones. The teratomas were formed via the subcutaneous injection of undifferentiated iPSCs into the posterior leg of NOD/SCID mice. VWM1: Open arrow, cartilage; asterisks, respiratory epithelia; arrow, muscle. VWM2: Arrowhead, adipocyte; asterisks, gut-like epithelia; open arrowhead, pigmented epithelia. The scale bar represents 200 μm . c, Karyotype analysis showed normal karyotypes of VWM iPSCs (more than 10 passages), 46, XY and 46, XX, respectively

2.6.4 | Differentiation into OL lineages

Neural stem cells were dissociated into single cells and transferred to a wall of a six-well plate coated with Matrigel at a density of $5 \times 10^4/\text{cm}^2$. The next day, the culture medium was changed to OL precursor

cell (OPC) medium (DMEM/F12: neural basal medium = 1:1 supplemented with $1 \times \text{N2}$, $1 \times \text{B27}$, $0.4 \mu\text{mol/L}$ SAG, 20 ng/mL bFGF, and 20 ng/mL PDGF-AA). After 7 days, the markers of NG2 and PDGFR α , which are indicative of OPCs, were detected by immunofluorescence assay. To differentiate the OPCs into OLs, the OPCs

FIGURE 3 Differentiation of iPSC-derived NSCs into neurons. a, Immunochemical analysis of iPSC-derived NSCs, NSCs were positive for Nestin and SOX2. b, Mean fluorescence densities of Nestin of NSCs, no significant difference exists, $P > 0.05$. c, Representative image of the immunochemistry of the NSC-derived neurons. The neurons were positive for β III-tubulin (green color) and Neurofilament H (red color) after 7 d of NSC differentiation. The scale bar represents 30 μm . d, Mean fluorescence densities of β III-tubulin and Neurofilament H of neurons; no significant difference exists, $P > 0.05$. e, Quantification of the early and total apoptosis of the neurons showed no significant differences between the Control, VWM1, and VWM2 neurons ($P > 0.05$, biological replicates, $n = 3$)



were dissociated into single cells and plate-cultured in a well of a six-well plate coated with Matrigel at a density of $5 \times 10^4/\text{cm}^2$. The next day, the culture medium was changed to an OL medium (DMEM/F12: neural basal medium = 1:1 supplemented with $1 \times \text{N2}$, $1 \times \text{B27}$, $0.4 \mu\text{mol/L}$ SAG, 30 ng/mL T3, 10 ng/mL NT3, $10 \mu\text{mol/L}$ cAMP, and 100 ng/mL IGF-1).¹³ MBP, indicative of mature OLs, was detected by immunofluorescence assay after the cells were cultured into OLs for 4 days.

2.7 | Apoptosis analysis

The cells were digested with trypsin without EDTA. According to the instructions of the apoptosis kit (Roche, Basel, Switzerland), $100 \mu\text{L}$ of binding buffer solution was added to each sample, mixed with $2 \mu\text{L}$ of Annexin V and $2 \mu\text{L}$ of PI, and light reaction was avoided for 15 minutes at room temperature. Apoptosis was detected by flow cytometry (BD, San Jose, CA, USA) within 1 hour and analyzed with FlowJo software (TreeStar, Ashland, OR, USA).

2.8 | Western blot analysis

For detecting total GFAP protein expression in astrocytes, total protein was extracted by RIPA buffer. Antibody to GFAP (mouse monoclonal, 1:500, CST) was used in routine Western blot analysis. The expression of GAPDH (mouse monoclonal, 1:1000) was used as a loading control.

2.9 | Statistical analysis

Statistical analysis was performed with SPSS 20.0 (Chicago, IL, USA). The ANOVA analysis was adopted to determine the statistical significance in the following assays: the number of processes and the length of the longest astrocytic process, apoptosis detection, fluorescence density, $P < 0.05$ was considered statistically significant.

2.10 | Ethical approval and consent forms

This study was approved by the clinical research ethics committee of the Peking University First Hospital, and informed consent forms were signed by the parents of the patients.

3 | RESULTS

3.1 | Phenotype and genotype of the two patients

Two VWM iPSC models (VWM1-iPSCs and VWM2-iPSCs), which are *EIF2B5* and *EIF2B3* compound heterozygous mutations, respectively, were established using a nonintegrating episomal vector system. Both patients were early childhood onset VWM, the developmental milestone before disease onset was normal. The first patient (VWM1) was a male, whose initial symptom was motor deterioration triggered by head trauma at 4 years old. At the last

follow-up in 2018, he was 16 years old and was bedridden. The second patient (VWM2) was a female, who was characterized by motor regression at the age of 3 and died at 12 years old. The brain MRI showed typical features of rarefaction of cerebral white matter (Figure 1a). The genotype of VWM1 was *EIF2B5*: c.1827_1838del (p. Ser610_Asp613del), c.1157G>A (P. Gly386Val); whereas the genotype of VWM2 was *EIF2B3*: c.140G>A (p. Gly47Glu), c.1037T>C (p. Ile346Thr) (Figure 1b).

3.2 | Establishment and characterization of the VWM HDFs-derived iPSCs

Forearm dermal tissue was obtained from the two VWM patients at the age of 10 and 11, respectively. To generate integration-free iPSCs, the Yamanaka episomal plasmids were electrotransfected into the HDFs of the two VWM patients using an Amaxa Nucleofector system. 25–30 days after electrotransfection, clones were picked and propagated under feeder-free conditions. iPSCs clones exhibited compact and flat appearance, similar to ESCs. In addition, iPSCs stained positive for alkaline phosphatase (ALP) staining and expressed typical pluripotent markers, SSEA4, and NANOG (Figure 2a). Furthermore, in vivo teratoma formation assay was performed in NOD SCID mice. After 2 months, teratomas were formed, and histological examination showed that the teratomas were composed of cells characterized by three germ layers (Figure 2b). Karyotype analysis showed that VWM1 and VWM2 iPSCs maintained normal karyotypes after 10 passages, namely, 46, XY and 46, XX, respectively (Figure 2c). Sanger sequencing confirmed that the VWM1 and VWM2 iPSCs carried the same mutations as the fibroblasts.

3.3 | VWM iPSCs differentiated into NSCs in vitro

Vanishing white matter disease iPSCs and two control iPSCs lines (C1 and C2) were induced to differentiate into NSCs by using neural induction medium. After two passages, both control and VWM iPSCs expressed Nestin and SOX2. Nestin was localized in the cytoplasm, whereas SOX2 was in the nuclei (Figure 3a). In addition, the mean fluorescence densities of Nestin in the C1, C2, VWM1, and VWM2 NSCs were 813.7, 805.5, 760.4, and 768.9, respectively, $P > 0.05$ (Figure 3b).

3.4 | VWM iPSC-derived NSCs differentiated into neurons in vitro

The control and VWM NSCs after two passages were induced to differentiate into neurons. On day 7, both β III-tubulin and Neurofilament H were positive in the control, VWM1, and VWM2 NSCs-derived neurons, and were localized in the cytoplasm (Figure 3c). In addition, the mean fluorescence densities of β III-tubulin in the C1, C2, VWM1, and VWM2 NSCs were 1375, 1388, 1393, and 1399, $P > 0.05$, whereas those of Neurofilament H were 814.8, 744.5, 841.3 and 831.5, respectively, $P > 0.05$ (Figure 3d).

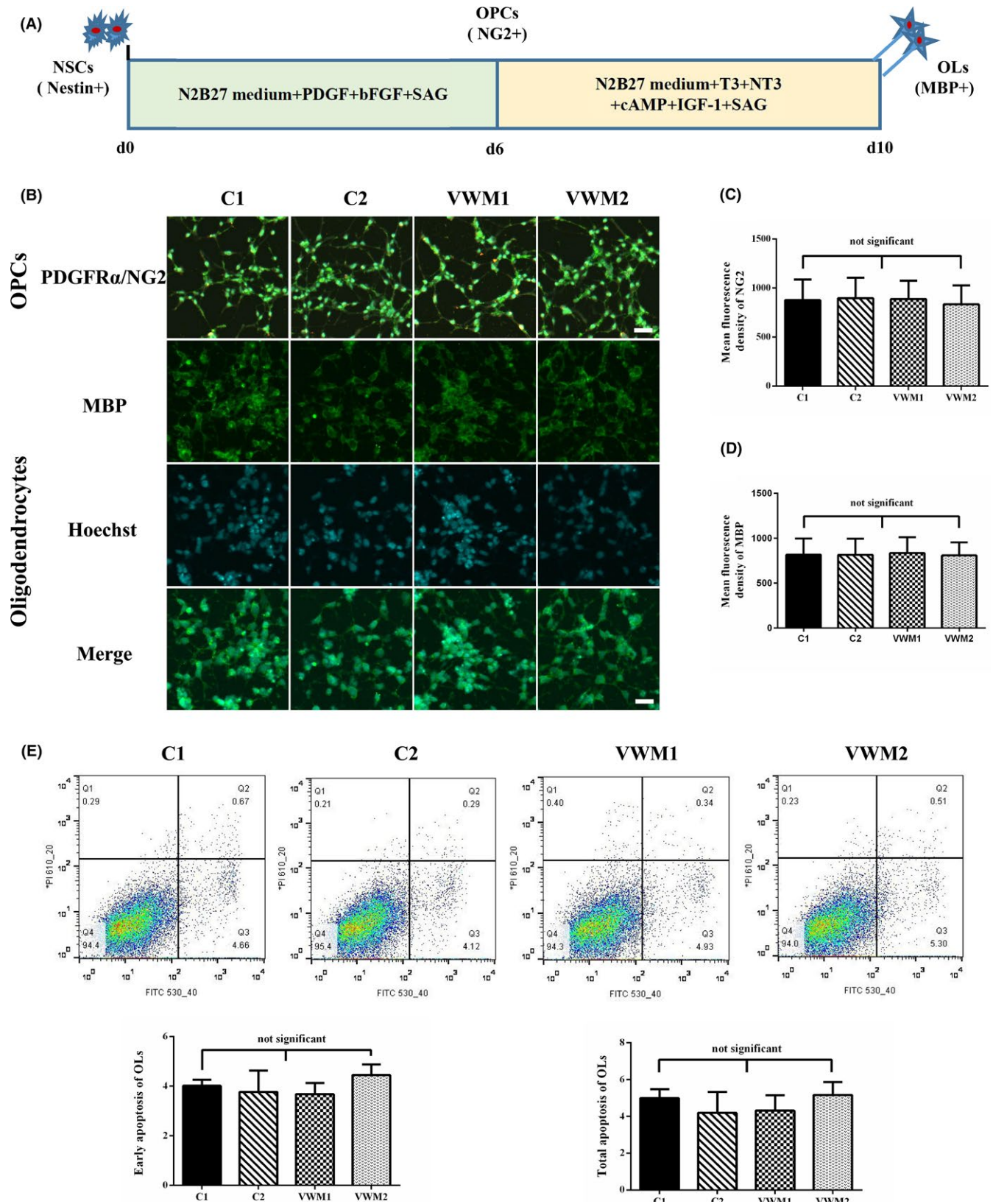
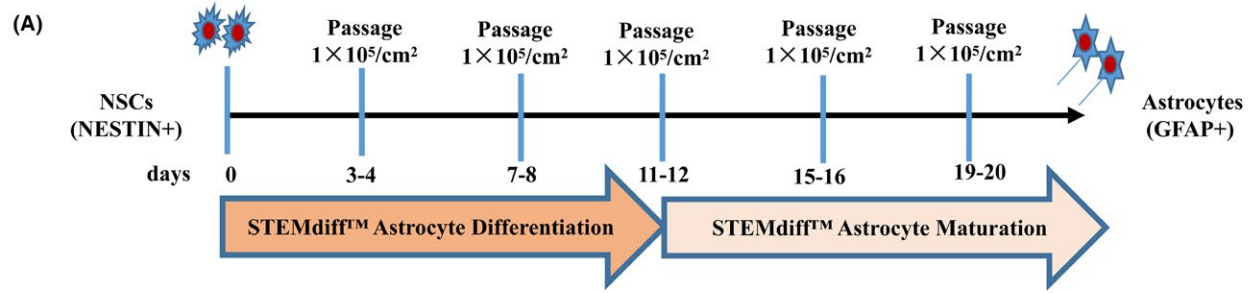
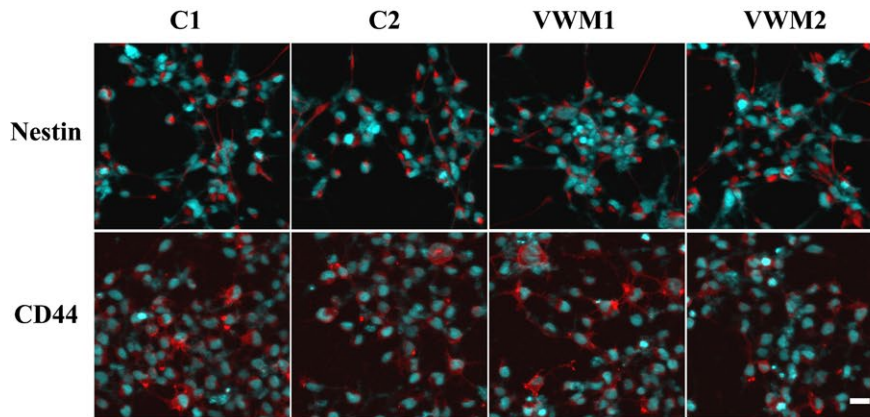


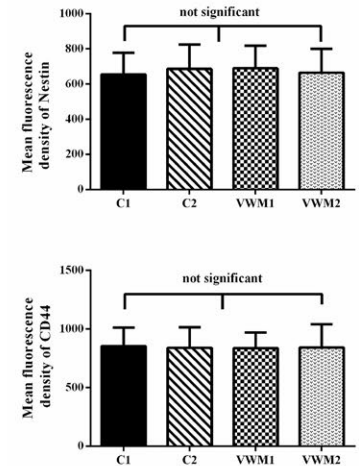
FIGURE 4 Differentiation of iPSC-derived NSCs into oligodendrocytes. a, Schematic presentation of the protocol for OLs differentiation from NSCs. b, Immunofluorescence analysis of iPSC-derived OPCs and OLs. Both control and VWM OPCs were positive for NG2 (green color) and PDGFRα (red color) after 6 d of NSCs differentiation. And both control and VWM OLs were positive for MBP after 4 d of OPCs differentiation. The scale bar represents 30 μm. c, d, Mean fluorescence densities of NG2 and MBP respectively; no significant difference exists, $P > 0.05$. e, Apoptosis detection of OLs via Annexin V/PI staining. Quantification of the early and total apoptosis of the OLs showed no significant differences between the controls, VWM1, and VWM2 OLs ($P > 0.05$, biological replicates, $n = 3$)



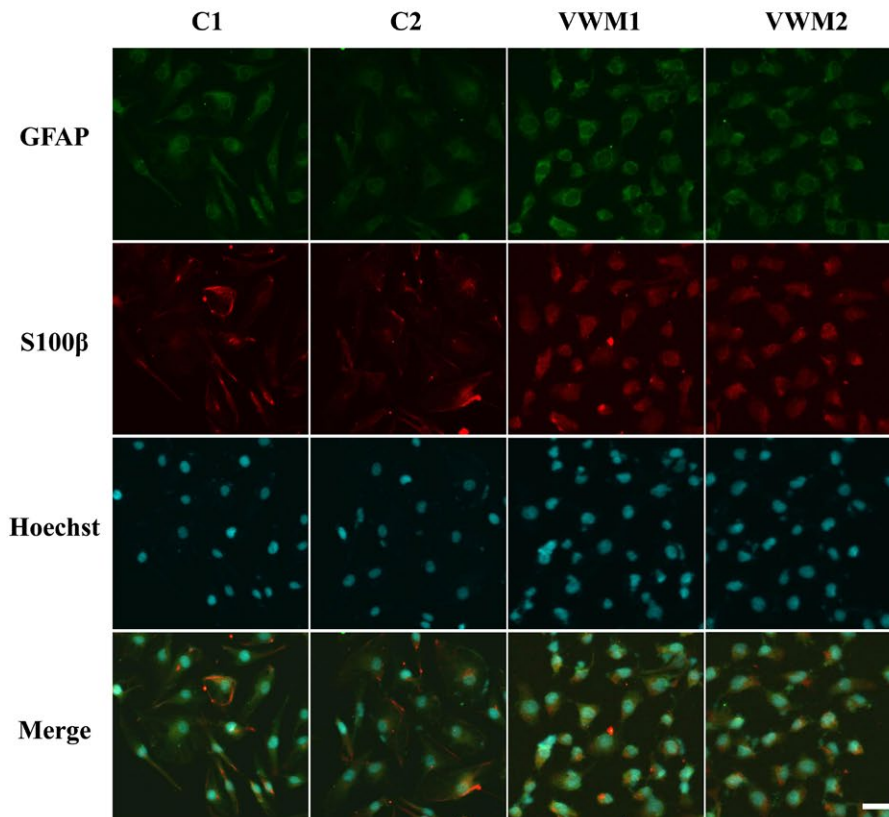
(B) Differentiation of astrocytes at day 8



(C)



(D) Differentiation of astrocytes at day 16



(E)

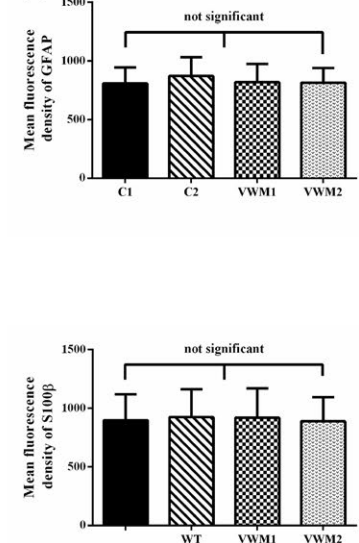


FIGURE 5 Differentiation of iPSC-derived NSCs into astrocytes. a, Schematic presentation of the protocol for astrocytes differentiation from NSCs. b, Cells were positive for Nestin and CD44 after 8 d of NSC differentiation into astrocytes. The scale bar represents 30 μm . c, Mean fluorescence densities of Nestin and CD44, respectively; no significant difference exists, $P > 0.05$. d, Both control and VWM Astrocytes were positive for GFAP (green color) and S100 β (red color) after 16 d of NSCs differentiation into astrocytes. The scale bar represents 30 μm . e, Mean fluorescence densities of GFAP and S100 β , respectively; no significant difference exists, $P > 0.05$

The apoptosis of neurons was further analyzed by AnnexinV/PI. The results revealed that the early apoptosis rates of the C1, C2, VWM1, and VWM2 neurons were 4.59%, 7.59%, 8.95%, and 7.36%, respectively, and their total apoptosis rates were 6.48%, 8.44%, 9.61%, and 9.96%, respectively. There is no significant difference in either early and total apoptosis rates between the controls and VWM neurons, $P > 0.05$ (Figure 3e).

3.5 | VWM iPSC-derived NSCs differentiated into OLs in vitro

The NSCs were differentiated into OLs by the standard protocol (Figure 4a). After the NSCs were cultured in the OPC medium for 7 days, OPCs derived from both control and VWM NSCs expressed PDGFR α and NG2 (Figure 4b). Both PDGFR α and NG2 were localized in the cytoplasm, the mean fluorescence densities of NG2 in C1, C2, VWM1, and VWM2 OPCs were 817.0, 815.3, 835.6, and 809.8 respectively ($P > 0.05$) (Figure 4c).

The OPCs were further differentiated into OLs. After 4 days, both the control and VWM OPCs expressed MBP, which was localized in the membrane (Figure 4b). The mean fluorescence densities of MBP in the C1, C2, VWM1, and VWM2 OLs were 817.0, 815.3, 835.5, and 809.7, respectively ($P > 0.05$) (Figure 4d).

The apoptosis of OLs was analyzed by AnnexinV/PI, which revealed that the early apoptosis rates of the C1, C2, VWM1, and VWM2 OLs were 4.66%, 4.12%, 4.93%, and 5.30%, respectively, and their total apoptosis rates were 5.33%, 4.41%, 5.27%, and 5.81%, respectively. No significant difference exists in early and total apoptosis rates between the controls, VWM1, and VWM2 OLs, $P > 0.05$ (Figure 4e).

3.6 | VWM iPSC-derived astrocytes exhibited abnormal morphology and increased apoptosis

3.6.1 | No difference found in the timing of markers in different stages of differentiation between control and VWM astrocytes

The NSCs were differentiated into astrocytes according to the standard protocol (Figure 5a). On day 8, both control and VWM cells expressed Nestin and CD44, indicative of astrocyte precursor cells (Figure 5b). Nestin was localized in the cytoplasm, and the mean fluorescence densities of Nestin in the C1, C2, VWM1, and VWM2 cells were 655.4, 686.3, 689.6 and 665.1, respectively ($P > 0.05$). CD44 was localized in the membrane, and the mean fluorescence densities of CD44 in the C1, C2, VWM1, and VWM2 cells were 856.1, 840.9, 838.1, and 843.4, respectively ($P > 0.05$) (Figure 5c). On day 16, both control and VWM cells expressed mature astrocytic markers GFAP and S100 β (Figure 5d),

both GFAP and S100 β were localized in the cytoplasm, and the mean fluorescence densities of GFAP in the C1, C2, VWM1, and VWM2 cells were 808.7, 871.7, 819.6, and 815.9 ($P > 0.05$), and those of S100 β were 897.9, 923.8, 918.9, and 889.6 ($P > 0.05$) (Figure 5e).

3.6.2 | VWM iPSC-derived astrocytes were dysmorphic

On day 28 of differentiation, the VWM1 and VWM2 astrocytes were significantly dysmorphic, manifested as relatively shorter processes (Figure 6a). The number of processes and the length of the longest astrocytic process were analyzed using phase contrast microscopy. The mean length of the longest process of the control astrocytes was 58.1 and 56.4 μm , whereas those of the VWM1 and VWM2 astrocytes were 37.1 and 39.5 μm , respectively ($P < 0.0001$). The numbers of processes between the control and VWM astrocytes did not demonstrate significant difference, $P > 0.1$ (Figure 6b).

3.6.3 | Overexpression of αB -Crystalline in VWM astrocytes

Increased expression of protein chaperon αB -crystalline was determined in VWM astrocytes (Figure 6c). αB -Crystalline positivity (αB -Crystalline/Hoechst) were further analyzed, and 100% of VWM1 and VWM2 astrocytes expressed αB -Crystalline compared with less than 5% of control astrocytes, $P < 0.0001$ (Figure 6d).

3.6.4 | Increased expression of δ -GFAP in VWM astrocytes

The GFAP expression in astrocytes was detected by RT-qPCR. The expression levels of total GFAP and α -GFAP in the VWM astrocytes were lower than those in the control astrocytes. By contrast, the expression levels of δ -GFAP in the VWM astrocytes were significantly higher than those in the control astrocytes, $P < 0.01$ (Figure 6e). The total GFAP expression in control and VWM astrocytes detected by Western blot exhibited no significant difference (Figure 6f).

3.6.5 | Increased apoptosis in VWM astrocytes

The apoptosis of astrocytes was detected on day 28 of differentiation. The early apoptosis rates of the C1, C2, VWM1, and VWM2 astrocytes were 14.6%, 15.0%, 17.1%, and 16.2%, respectively, and their total apoptosis rates were 16.8%, 17.9%, 21.0%, and 20.0%, respectively. Both the early and total apoptosis rates of the VWM astrocytes were higher than those of the control astrocytes, $P < 0.05$ (Figure 6g).

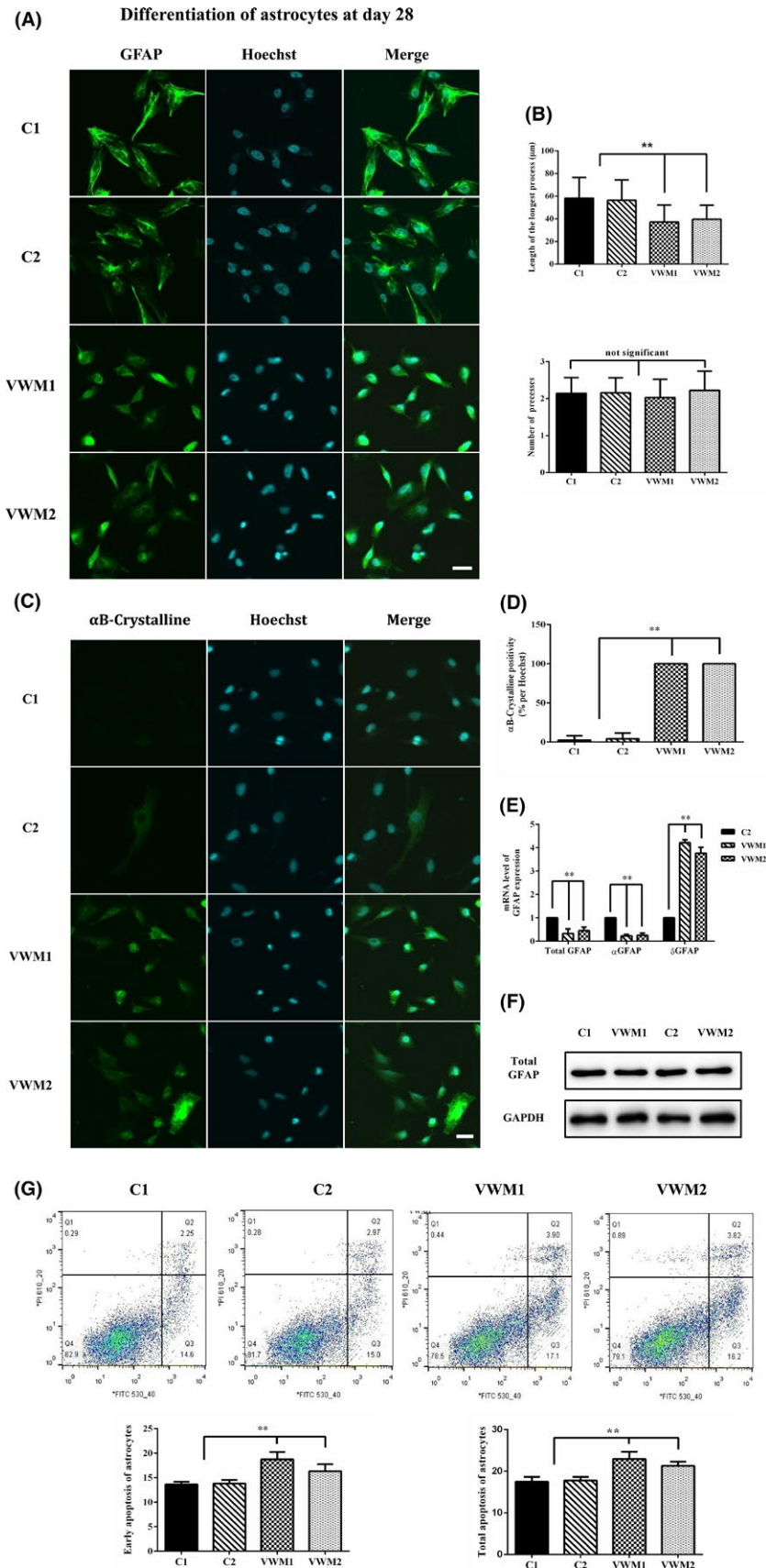


FIGURE 6 Involvement of VWM iPSC-derived astrocytes. a, Representative image of the immunocytochemistry of control and VWM astrocytes. The mature astrocytes were positive for GFAP after 28 d of NSCs differentiation into astrocytes. The scale bar represents 30 μm . b, Calculated length of the longest astrocytic process and number of processes of the astrocytes (10 fields were randomly selected, with at least 8 cells in each field). c, Immunocytochemical analysis of the expression of $\alpha\text{B-Crystalline}$ in control and VWM astrocytes. The scale bar represents 30 μm . d, Calculated positivity of $\alpha\text{B-Crystalline}$ -positive ($\alpha\text{B-Crystalline}/\text{Hoechst}$) astrocytes (**, $P < 0.0001$, 10 fields were randomly picked, with at least 8 cells in each field). e, Real-time quantitative PCR analysis for GFAP (total, αGFAP and $\delta\text{-GFAP}$) expression in Control and VWM astrocytes (**, $P < 0.01$ in the three groups, biological replicates, $n = 3$). f, The total GFAP expression in Control and VWM astrocytes detected by Western blot exhibited no significant difference. g, Apoptosis detection in the astrocytes via Annexin V/PI staining and quantification of total and early apoptosis of astrocytes (** represents $P < 0.01$, * represents $P < 0.05$, biological replicates, $n = 3$)

Overall, compared with the control astrocytes, the VWM astrocytes exhibited abnormal morphology, expressed abnormal antigenic phenotypes, and manifested increased total and early apoptosis, suggesting that VWM astrocytes were dysfunctional and involved in the pathogenesis of VWM.

4 | DISCUSSIONS

4.1 | Advantages and disadvantages of disease models of VWM

The exact pathogenesis of VWM remains unknown. Current studies of VWM mainly concentrated in the following aspects: the overactivation of unfolded protein reaction (UPR), mitochondrial dysfunction, and glial maturation dysfunction.^{9,14-17} Previous studies mainly used patients' postmortem brain tissue, animal models, or cell transfection. The postmortem brain tissue VWM patients can reflect the pathological features at the tissue and cellular levels. However, the brain tissue is usually difficult to obtain, and can only reflect the terminal state rather than the dynamic changes in the disease. Animal models are more readily available and can be used for multilevel studies, but the phenotypes of mice and VWM patients are not completely parallel.^{18,19} Currently, *in vitro* virus-mediated cell transfection is widely used; however, viral genome may be randomly integrated into the host cell genome. In addition, the overexpression of target gene could not reflect the physiological situation or maintain stable transfection.^{22,23} In our study, VWM disease-specific iPSC models were established for the first time, however, several main disadvantages of iPSC models such as new variants, epigenetic modification, and tumor formation remain unsolved, which prevent utilization of iPSCs in clinical application like *in vivo* transplantation.

4.2 | VWM glial cells are selectively involved, but neurons are spared

The typical brain MRI of VWM patients shows that the cerebral white matter is diffusely rarefied, whereas the cortex is relatively well preserved.^{7,24,25} In addition, the histomorphology of the postmortem brain tissue of VWM patients and mouse models suggested that myelin is lost, and white matter is liquefied or vacuolated, whereas the gray matter looks normal. Histopathological evaluation indicated that astrocytes show abnormal morphology and decreased reactive gliosis, increased foaming OLs and apoptosis, whereas neurons are relatively normal.^{27,28} In the current study, VWM iPSC-derived NSCs could normally differentiate into neurons, further supporting that neurons are spared in VWM.

4.3 | Astrocytes may play a central role in the pathogenesis of VWM

In the central nervous system (CNS), astrocytes account for the largest number of cells and play a central role in the maintenance of homeostasis, the response to injury, and the pathogenesis of disease.

Astrocytes participate in a series of complex pathological processes, such as reactive gliosis, antioxidant, and immune regulation.^{30,31}

Several studies have suggested that astrocytes are central in the pathogenesis of VWM. Dietrich et al³³ cultured astrocytes and OLs *in vitro* from the brain tissue of a VWM patient with *EIF2B5* mutation; they found that few GFAP+astrocytes were present and astrocytic induction was severely compromised, whereas normal OLs can be cultured. Detailed VWM pathological examination has revealed meager reactive astrogliosis, dysmorphic astrocytes, and increased expression of delta isoform GFAP (δ -GFAP) and heat shock protein α B-crystalline.³⁴ Although *in vitro* evidence has confirmed that astrocytes are primarily impaired, the postmortem brain tissue and animal models of VWM have suggested that OLs are also involved, showing that the OLs are foamy and the number of myelin-forming OLs were decreased.^{3,27,34,35} In addition, Van Haren et al³⁷ found that OLs increased in number but also demonstrated limited proliferation and increased apoptosis in VWM. We also found in our previous studies that OLs transfected with mutant eIF2B showed ERS intolerance, overactivation of UPR and decreased autophagy.^{38,39}

In our study, we found that VWM iPSC-derived NSCs can normally differentiate into OPCs, and OLs *in vitro*. Whereas, VWM iPSC-derived astrocytes were dysmorphic, expressed a significant increased δ -GFAP and α B-Crystalline, and showed increased early and total apoptosis as well, which indicating the astrocytic dysfunction. Dysmorphic astrocytes overexpressed δ -GFAP, suggesting that the intermediate fiber network of VWM astrocytes was affected, resulting in abnormal morphology and meager astrogliosis.^{3,40} Previous studies showed that astrocytes can influence OPC survival, differentiation, and maturation.^{41,42} Typical neuropathological findings showed that axons are lost in cavitated white matter and remaining axons are abnormally thin. Klok, et al⁴⁵ proposed that axons are initially normal and atrophy later in VWM, and astrocytes are central in this process. Bugiani et al^{34,46} found myelin vacuolation and increased density of OPCs with normal proliferation in the brain tissue of VWM patients, whereas VWM astrocytes inhibited the differentiation of OPCs into mature myelin-forming OLs. Dooves et al⁴⁷ found in their coculture experiments that VWM astrocytes could inhibit the maturation of wild-type OLs. Therefore, mutant astrocytes may play a major role in the vanishing of white matter by disturbance of function and survival of OLs. In the newly proposed classification system of leukodystrophy, VWM was classified as an astrocytic disease.⁴⁸

In addition to the pathological changes in astrocytes in cerebral white matter, astrocytes in other regions can also be involved. Both in VWM patients and mouse model of VWM, Bergmann glia in the cerebellum and Müller cells in the retina are also affected. The Bergmann glia in the cerebellum shows mislocalization to the molecular layer, and the involvement of Müller glia was manifested as retinal dysplasia. Retrospective evaluation of patients' electroretinographic data confirmed that retinopathy is also a sign of VWM patients.^{40,47} Moreover, Leferink et al⁴⁹ also identified astrocytic abnormalities in the spinal cord of a mouse model for VWM and the postmortem tissue of two VWM patients.

4.4 | Limitations

There must be some differences between iPSC differentiation in vitro and neural differentiation in vivo. Moreover, although iPSCs carry VWM mutations, new variants, and epigenetic changes may occur during the processes of iPSCs reprogramming and differentiation.

5 | CONCLUSIONS

In this study, two VWM iPSC models were established using a virus-free nonintegrating episomal vector system for the first time. The results suggested that there was no difference in the in vitro differentiation of control and VWM iPSCs into NSCs, neurons, and OLs. Whereas, VWM astrocytes exhibited abnormal morphology, increased expression of δ -GFAP and α B-Crystalline, and increased early and total apoptosis, further supporting that astrocytes may play a central role in the pathogenesis of VWM. In addition, the established VWM-specific iPSCs models provide a platform for further study on the pathogenesis and future drug screening.

ACKNOWLEDGMENTS

This work was supported by the National Natural Science Foundation of China (81741053, 81601131, 81501123), Beijing Natural Science Foundation (7151010, 7172217), Beijing Municipal Science & Technology Commission (Z16110000216133, Z161100004916169), Beijing Institute for Brain Disorders Foundation (BIBDPXM2014_014226_000016), Beijing Municipal Natural Science Key Project (15G10050), Beijing key laboratory of molecular diagnosis and study on pediatric genetic diseases (BZ0317), National Key Research and Development Program of China (2016YFC1306201, 2016YFC0901505), Clinical Medicine Plus X project of Peking University, Fundamental Research Funds for the Central Universities (BMU2017J1002, BMU2018XY006, PKU2017LCX06), the Public Foundation of Beijing Center of Neural Regeneration and Repair, the construction of a clinical evaluation platform for demonstration new drug for children's rare disease (2017ZX09304029-006).

CONFLICT OF INTEREST

The authors declare no conflict of interest.

ORCID

Ling Zhou  <https://orcid.org/0000-0002-8221-2917>

REFERENCES

1. Takahashi K, Tanabe K, Ohnuki M, et al. Induction of pluripotent stem cells from adult human fibroblasts by defined factors. *Cell*. 2007;131(5):861-872.
2. van der Knaap MS, Pronk JC, Scheper GC. Vanishing white matter disease. *Lancet Neurol*. 2006;5(5):413-423.
3. Bugiani M, Boor I, Powers JM, Scheper GC, van der Knaap MS. Leukoencephalopathy with vanishing white matter: a review. *J Neuropathol Exp Neurol*. 2010;69(10):987-996.
4. Kaczorowska M, Kuczynski D, Jurkiewicz E, Scheper GC, van der Knaap MS, Jozwiak S. Acute fright induces onset of symptoms in vanishing white matter disease-case report. *Eur J Paediatr Neurol*. 2006;10(4):192-193.
5. Prange H, Weber T. Vanishing white matter disease: a stress-related leukodystrophy. *Nervenarzt*. 2011;82(10):1330-1334.
6. van der Knaap MS, Leegwater PA, Könst AA, et al. Mutations in each of the five subunits of translation initiation factor eIF2B can cause leukoencephalopathy with vanishing white matter. *Ann Neurol*. 2002;51(2):264-270.
7. Leegwater PA, Pronk JC, van der Knaap MS. Leukoencephalopathy with vanishing white matter: from magnetic resonance imaging pattern to five genes. *J Child Neurol*. 2003;18(9):639-645.
8. Pronk JC, vanKollenburg B, Scheper GC, van der Knaap MS. Vanishing white matter disease: a review with focus on its genetics. *Ment Retard Dev Disabil Res Rev*. 2006;12(2):123-128.
9. Scheper GC, Proud CG, van der Knaap MS. Defective translation initiation causes vanishing of cerebral white matter. *Trends Mol Med*. 2006;12(4):159-166.
10. Fontes A, MacArthur CC, Lieu PT, Vemuri MC. Generation of human-induced pluripotent stem cells (hiPSCs) using episomal vectors on defined essential 8 medium conditions. *Methods Mol Biol*. 2013;997:57-72.
11. Li P, Sun X, Ma Z, et al. Transcriptional reactivation of OTX2, RX1 and SIX3 during reprogramming contributes to the generation of RPE cells from human iPSCs. *Int J Biol Sci*. 2016;12(5):505-517.
12. Schlaeger TM, Daheron L, Brickler TR, et al. A comparison of non-integrating reprogramming methods. *Nat Biotechnol*. 2015;33(1):58-63.
13. Eliott MS, Shick HE, Madhavan M, et al. Chemical screening identifies enhancers of mutant oligodendrocyte survival and unmasks a distinct pathological phase in pelizaeus-merzbacher disease. *Stem Cell Reports*. 2018;11(3):711-726.
14. van der Voorn JP, van Kollenburg B, Bertrand G, et al. The unfolded protein response in vanishing white matter disease. *J Neuropathol Exp Neurol*. 2005;64(9):770-775.
15. Elroy-Stein O. Mitochondrial malfunction in vanishing white matter disease: a disease of the cytosolic translation machinery. *Neural Regen Res*. 2017;12(10):1610-1612.
16. Raini G, Sharef R, Herrero M, et al. Mutant eIF2B leads to impaired mitochondrial oxidative phosphorylation in vanishing white matter disease. *J Neurochem*. 2017;141(5):694-707.
17. van Kollenburg B, van Dijk J, Garbern J, et al. Glia-specific activation of all pathways of the unfolded protein response in vanishing white matter disease. *J Neuropathol Exp Neurol*. 2006;65(7):707-715.
18. Geva M, Cabilly Y, Assaf Y, et al. A mouse model for eukaryotic translation initiation factor 2B-leucodystrophy reveals abnormal development of brain white matter. *Brain*. 2010;133(Pt 8):2448-2461.
19. Cabilly Y, Barbi M, Geva M, et al. Poor cerebral inflammatory response in eIF2B knock-in mice: implications for the aetiology of vanishing white matter disease. *PLoS ONE*. 2012;7(10):e46715.
20. Gat-Viks I, Geiger T, Barbi M, Raini G, Elroy-Stein O. Proteomics-level analysis of myelin formation and regeneration in a mouse model for vanishing white matter disease. *J Neurochem*. 2015;134(3):513-526.
21. Wisse LE, Ter Braak TJ, van de Beek MC, et al. Adult mouse eIF-2Bepsilon Arg191His astrocytes display a normal integrated stress response in vitro. *Sci Rep*. 2018;8(1):3773.
22. Hahn P, Scanlan E. Gene delivery into mammalian cells: an overview on existing approaches employed in vitro and in vivo. *Top Curr Chem*. 2010;296:1-13.

23. Stepanenko AA, Heng HH. Transient and stable vector transfection: pitfalls, off-target effects, artifacts. *Mutat Res*. 2017;773:91-103.
24. van der Lei HD, Steenweg ME, Barkhof F, et al. Characteristics of early MRI in children and adolescents with vanishing white matter. *Neuropediatrics*. 2012;43(1):22-26.
25. Meoded A, Poretti A, Yoshida S, Huisman TA. Leukoencephalopathy with vanishing white matter: serial MRI of the brain and spinal cord including diffusion tensor imaging. *Neuropediatrics*. 2011;42(2):82-85.
26. Harder S, Gourgaris A, Frangou E, et al. Clinical and neuroimaging findings of Cree leukodystrophy: a retrospective case series. *AJNR Am J Neuroradiol*. 2010;31(8):1418-1423.
27. Rodriguez D, Gelot A, della Gaspera B, et al. Increased density of oligodendrocytes in childhood ataxia with diffuse central hypomyelination (CACH) syndrome: neuropathological and biochemical study of two cases. *Acta Neuropathol*. 1999;97(5):469-480.
28. Topcu M, Saatci I, Anil Apak R, Söylemezoglu F. A case of leukoencephalopathy with vanishing white matter. *Neuropediatrics*. 2000;31(2):100-103.
29. Hata Y, Kinoshita K, Miya K, et al. An autopsy case of infantile-onset vanishing white matter disease related to an EIF2B2 mutation (V85E) in a hemizygous region. *Int J Clin Exp Pathol*. 2014;7(6):3355-3362.
30. Sofroniew MV, Vinters HV. Astrocytes: biology and pathology. *Acta Neuropathol*. 2010;119(1):7-35.
31. Davila D, Thibault K, Fiocco TA, Agulhon C. Recent molecular approaches to understanding astrocyte function in vivo. *Front Cell Neurosci*. 2013;7:272.
32. Almad A, Maragakis NJ. A stocked toolbox for understanding the role of astrocytes in disease. *Nat Rev Neurol*. 2018.
33. Dietrich J, Lacagnina M, Gass D, et al. EIF2B5 mutations compromise GFAP+ astrocyte generation in vanishing white matter leukodystrophy. *Nat Med*. 2005;11(3):277-283.
34. Bugiani M, Boor I, van Kollenburg B, et al. Defective glial maturation in vanishing white matter disease. *J Neuropathol Exp Neurol*. 2011;70(1):69-82.
35. Bruck W, Herms J, Brockmann K, Schulz-Schaeffer W, Hanefeld F. Myelinopathia centralis diffusa (vanishing white matter disease): evidence of apoptotic oligodendrocyte degeneration in early lesion development. *Ann Neurol*. 2001;50(4):532-536.
36. Wong K, Armstrong RC, Gyure KA, et al. Foamy cells with oligodendroglial phenotype in childhood ataxia with diffuse central nervous system hypomyelination syndrome. *Acta Neuropathol*. 2000;100(6):635-646.
37. Van Haren K, van der Voorn JP, Peterson DR, van der Knaap MS, Powers JM. The life and death of oligodendrocytes in vanishing white matter disease. *J Neuropathol Exp Neurol*. 2004;63(6):618-630.
38. Chen N, Dai L, Jiang Y, et al. Endoplasmic reticulum stress intolerance in EIF2B3 mutant oligodendrocytes is modulated by depressed autophagy. *Brain Dev*. 2016;38(5):507-515.
39. Chen N, Jiang YW, Hao HJ, et al. Different eukaryotic initiation factor 2Bepsilon mutations lead to various degrees of intolerance to the stress of endoplasmic reticulum in oligodendrocytes. *Chin Med J (Engl)*. 2015;128(13):1772-1777.
40. Bugiani M, Vuong C, Breur M, van der Knaap MS. Vanishing white matter: a leukodystrophy due to astrocytic dysfunction. *Brain Pathol*. 2018;28(3):408-421.
41. Sakurai Y, Nishimura D, Yoshimura K, Tsuruo Y, Seiwa C, Asou H. Differentiation of oligodendrocyte occurs in contact with astrocyte. *J Neurosci Res*. 1998;52(1):17-26.
42. Schnadelbach O, Fawcett JW. Astrocyte influences on oligodendrocyte progenitor migration. *Prog Brain Res*. 2001;132:97-102.
43. Carmen J, Magnus T, Cassiani-Ingoni R, Sherman L, Rao MS, Mattson MP. Revisiting the astrocyte-oligodendrocyte relationship in the adult CNS. *Prog Neurobiol*. 2007;82(3):151-162.
44. Domingues HS, Portugal CC, Socodato R, Relvas JB. Oligodendrocyte, astrocyte, and microglia crosstalk in myelin development, damage, and repair. *Front Cell Dev Biol*. 2016;4:71.
45. Klok MD, Bugiani M, de Vries SI, et al. Axonal abnormalities in vanishing white matter. *Ann Clin Transl Neurol*. 2018;5(4):429-444.
46. Bugiani M, Postma N, Polder E, et al. Hyaluronan accumulation and arrested oligodendrocyte progenitor maturation in vanishing white matter disease. *Brain*. 2013;136(Pt 1):209-222.
47. Dooves S, Bugiani M, Postma NL, et al. Astrocytes are central in the pathomechanisms of vanishing white matter. *J Clin Invest*. 2016;126(4):1512-1524.
48. van der Knaap MS, Bugiani M. Leukodystrophies: a proposed classification system based on pathological changes and pathogenetic mechanisms. *Acta Neuropathol*. 2017;134(3):351-382.
49. Leferink PS, Breeuwsma N, Bugiani M, van der Knaap MS, Heine VM. Affected astrocytes in the spinal cord of the leukodystrophy vanishing white matter. *Glia*. 2018;66(4):862-873.

How to cite this article: Zhou L, Li P, Chen N, et al. Modeling vanishing white matter disease with patient-derived induced pluripotent stem cells reveals astrocytic dysfunction. *CNS Neurosci Ther*. 2019;25:759-771. <https://doi.org/10.1111/cns.13107>